J. Environ. Nanotechnol.
Volume 4, No.1 (2015) pp. 65-74
ISSN (Print): 2279-0748
ISSN (Online): 2319-5541
doi:10.13074/jent.2015.03.152146

Growth, Spectral, Structural and Thermal Properties of Inorganic Materials TetrabutylammoniumTetrabromoCobaltate (II) Crystal

R. Umarani[1*], V. Mohanraj[2], M. Thenmozhi[3], M. A. Kandasamy[4]

[1]Department of Chemistry, Government Arts College (Autonomous), Coimbatore, TN, India.*
[2,4]Department of Chemistry, SRMV College of Arts and Science (Autonomous), Coimbatore, TN, India.
[3]Centre for Nanotechnology and Advanced Biomaterials, SASTRA University, Thanjavur, TN, India.

Received: 22.04.2015 Accepted: 08.05.2015

Abstract

Single crystals of Tetrabutylammoniumtetrabromocobaltate (II) crystal, was grown by slow evaporation method at room temperature. The crystals belong to a class of compounds that shown interesting properties like phase transitions and ferroelectric behaviour in a narrow temperature. The grown crystals were characterized through elemental analysis, powder X-ray diffraction, thermogravimetric analysis, differential thermal analysis, low temperature differential scanning calorimetry techniques. The spectral studies of FTIR, ^{1}H and ^{13}C NMR spectra were obtained for the sample. Single crystal X-ray diffraction technique is used to find the structure and crystal packing of the compounds.

Keywords: *Crystal growth; NMR Spectroscopy; Single crystal X-ray diffraction; Tetrabutylammoniumtetrabromocobaltate (II); Thermogravimetric analysis.*

1. INTRODUCTION

Crystal growth involves phase transformation of materials of interest from solid, liquid or gaseous phase to a well ordered solid phase resulting in a crystal (Sawada *et al.* 1995; Iwata *et al.* 1991). Orderly arranged atoms, ions or molecules in crystalline solids provide shining appearance and coloured crystals are still more attractive. The art of growing crystals has always been fascinating and challenging. Modern technology employing semiconductors, magnetic garnets and solid state lasers ultraviolet and infrared requires materials in good crystalline form (Kahrizi *et al.* 1990). Solid state electronics has become the key to modern technology and its importance is likely to keep growing. Monocrystalline silicon is used in electronics for logic control and power devices. The growth of crystals containing two or more components plays an important role in several modern industrial applications (Young *et al.* 1998; Byrappa *et al.* 1999; Amirthaganesan *et al.* 2003; Moore *et al.* 2005; Koopmans *et al.* 1993).

***R. Umarani** *Tel. no: +919080840066*
Email : grishchandru@yahoo.com

An essential feature of the members of the above group is that they undergo several phase transition, both commensurate and incommensurate. Phase transitions and ferroelectric behaviour in a narrow temperature range in the commensurate phase (Shuai *et al.* 1994; Eychmuller *et al.* 2000). The occurrence of incommensuratephase crystals makes their study interesting. Most of the crystals in this family are isomorphous. Alkyl substituted ammonium derivative crystals of the type A_2BX_4 (Where A= Univalent cation, B= Divalent transition metal cation and X=Halogen) exhibit phase transitions mainly due to the rotational and conformational motion of the alkyl groups (Petrosyan *et al.* 2005; Xue *et al.* 2005). Alkyl substituted ammonium derivatives of A_2BX_4 type compounds have been extensively investigated in recent years (Maurya *et al.* 2003). Tetraalkylammoniumtetrahalometallates undergo several phase transitions, the most interesting one is the incommensurate phase occurring around 281K,

$$2[N(C_4H_9)4]Br + CoBr_2 \xrightarrow{H2O} [N(C_4H_9)_4]_2CoBr_4$$

Scheme - 1: Reaction of Tetrabutylammonium tetrabromo cobaltate (II)

A survey of literature shows that the compound, Tetrabutyl ammoniumtetrabromocobaltate (II) crystals, has not been synthesised so far. This paper deals with the synthesis and a preliminary study of the compound. The compound was characterised through single crystal X-ray diffraction, powder XRD, TG-DTA, DSC, low temperatures DSC, NMR and FTIR spectroscopy.

2. EXPERIMENTAL

2.1 Preparation and Crystal Growth

Single crystals of tetrabutylammoniumtetrabromocobaltate (II) crystal [TBATBr-Co(II)], were grown by slow evaporation method at room temperature. The equation is as follows Scheme 1. Aqueous solutions of analar grade (E Merck) tetrabutylammonium bromide and cobalt bromide were prepared separately in 2:1 molar ratio using triply distilled water. The two solutions were mixed thoroughly. In order to maintain acidic medium and to avoid hydrolysis then 1 ml of HBr is added. The resulting solution was filtered using Whatmann paper 42. The filtrate collected in a beaker was covered by filter paper with minute pores and kept for growth of crystals care was taken to minimize temperature gradient and mechanical shock at the place of crystal growth.

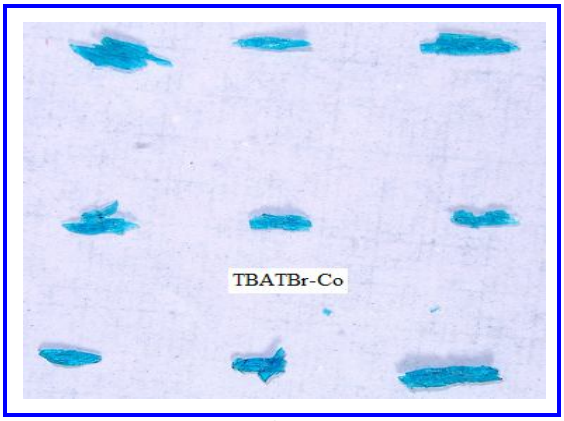

Fig. 1: The photograph of the grown TBATBr-Co(II) crystals

3. CHARACTERISATION TECHNIQUES

The powder XRD reveals the structure of the crystal is monoclinic with space group $P2_1/n$. The FTIR spectrum of the sample was recorded in the frequency region of 400-4000 cm^{-1} by employing Perkin Elmer FTIR spectrometer (model Spectrum RX1) using the KBr pellet. The ^1H NMR spectrums was recorded on in AVANCE III 500 MHz Bruker spectrometer using tetra methyl silane (TMS) as the internal reference. Simultaneous thermo gravimetric analysis (TGA) and differential thermal analysis (DTA) were carried out for the crystals using Seiko thermal analyzer.

3.1 Elemental Analysis

Elemental analysis of TBATBr-Co(II) was carried out in an ELEMENTAR VARIO ELIII instrument. In the order to conform the chemical composition of the synthesized complex C, H and N analysis was carried out. The experimental and calculated percentage of carbon, nitrogen, and hydrogen are given in Table 1. The difference and calculated percentages of carbon, nitrogen, and nitrogen are very close to each other and within the experimental errors. This confirms the formation of the complex in the stoichiometric proportion.

Table 1. Elemental analysis of TBATBr-Co(II)

Compound	C%		H%		N%	
	Exp	Theo	Exp	Theo	Exp	Theo
TBATBr-Co(II)	43.45	44.50	8.96	8.34	3.15	3.24

3.2 Infrared Spectroscopy

The FTIR spectra of the TBATBr-Co(II) crystals was carried out using Perkin Elmer model RX1 spectrometer employing KBr pellet technique. The FTIR spectrum is shown in Fig. 2.

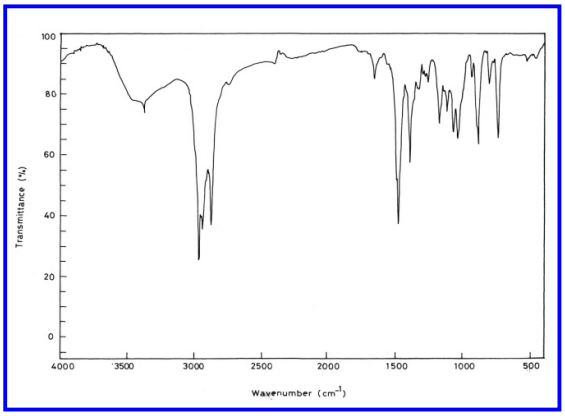

Fig. 2: FT-IR spectrum of TBATBr-Co(II)

The absorption frequencies and assignments to their respective vibrational modes are presented in Table 2. The broad band around 3376 cm^{-1} is due to the trapped water molecules in the crystal. No strong band is observed above 3000 cm^{-1} excluding the presence of groups like -OH, $-NH_2$, -NHR, HC=C-R, R_2C=CHR, aromatic system. It confirms the presence of nitrogen in tertiary or quaternary state. The band at 2959 cm^{-1} is due to C-H asymmetric stretching vibration of methyl group. The band at 2932 cm^{-1} is owing to C-H asymmetric stretching vibration of methylene group. The δ asymmetric stretching vibration of methyl and methylene groups is seen at 2872 cm^{-1} and 2700 cm^{-1} respectively.

Table 2. IR spectral data and assignments of TBATBr-Co(II)

Wave Number (cm-1)	Assignment
3376	Broad band shows presence of moisture in the compound
2959	Asymmetric stretching due to CH3
2932	Asymmetric stretching of methylene group
2872	Symmetric stretching of methyl group
2700	Symmetric stretching of methylene group
1637	Asymmetric bending vibration of O-H group
1467	Methyl and methylene asymmetric deformation
1379	C-H in-plane symmetric bending vibration of methyl group
1244	CH2 twisting mode
1165	CH3 twisting mode
1107	CH3 rocking mode.
1065	CH2 rocking mode.
1032	Γ asymmetric C-C-N
926	Γ asymmetric C-N-C
880	symmetric C-C stretching vibration
803	C-H out of plane bending mode
740	CH2 inplane bending vibration, C-C-N and C-N-C deformation modes

Weak band at 1637 cm^{-1} is caused by asymmetric bending vibration of O-H group. Band at 1467 cm^{-1} is due to methyl and methylene asymmetric deformation. C-H in plane symmetrical bending vibration of methyl group is observed as a strong band at 1379 cm^{-1}. This band is because of methyl group and not methylene group. A common feature of IR spectra is that groups like $-CH_3$, $-CH_2$, -CH have more or less the same frequency irrespective of molecular environment. These groups vibrate independently from the rest of the molecule. These frequencies are known as group frequencies. The C-C stretching vibrations are weak, which appear in the broad region between 1200 cm^{-1} and 800 cm^{-1} and it is not so useful. C-H stretching and bending vibrations are useful. Twisting and wagging are of less diagnostic value because of their instability. The instability is caused by strong coupling to the remainder of the molecule. Overtone of C-H bending is also observed as weak band in this region. Because of these reasons weak bands appear in the IR spectra between 1150 cm^{-1} and 803 cm^{-1}. The methylene and methyl twisting modes are observed as weak bands at 1244 cm^{-1} and 1165 cm^{-1}, respectively. Methyl and methylene rocking modes are observed at 1107 cm^{-1} and 1065 cm^{-1}, respectively. Bands appear at 1032 cm^{-1} and 926 cm^{-1} which are attributable to C-C-N and C-N-C stretching vibrations (Table 2). The bands also confirm the presence of unconjugated C-C-N linkage in the compound. The symmetrical stretching C-C vibration is observed at 880 cm^{-1}.C-H out of plane bending mode appears at 803 cm^{-1}. CH_2 in-plane bending vibration is found at 740 cm^{-1}. The peak is also due to C-C-N and C-N-C deformation vibration.

3.3 ^{1}H NMR Spectral Analysis

The proton NMR spectrum of TBATBr-Co(II) was recorded in AVANCE III 500 MHz Bruker Facility. The ^{1}H NMR spectrum is shown in Fig. 3. In this spectrum, four different signals are observed at different δ values for the methyl and methylene groups present in the butyl groups of the compound. The expected δ values for methylene and methyl protons are 1.2 to 1.4 ppm and 0.7 to 1.1 ppm, respectively. In this NMR spectrum higher δ value is obtained. This is due to the deshielding effect which confirms the presence of positive charge on the nitrogen of tetrabutylammonium group. The NMR spectrum cannot be taken for the negative ion $(CoBr_4)^{2-}$ because of the absence of hydrogen. The signal at -0.836 δ is due to methyl group protons (I). Peak at 1.3 δ is due to methylene protons (II). The signal for methylene protons (III) appear at 1.560 δ. The methylene protons (IV) signal appears at a higher δ value of 3.160. The higher δ value is due to deshielding effect because of the electropositive nitrogen adjacent to it. The deshielding effect decreases as we go from methylene protons (IV) to methyl protons (I). This is because the distance between nitrogen and the protons increases resulting in diminishing deshielding effect. Also, the intensity of the peak is higher for methyl protons (I) and the intensity of all other peaks are similar confirming the presence of three methylene groups in the compound.

All the butyl groups are in the same magnetic and chemical environment.

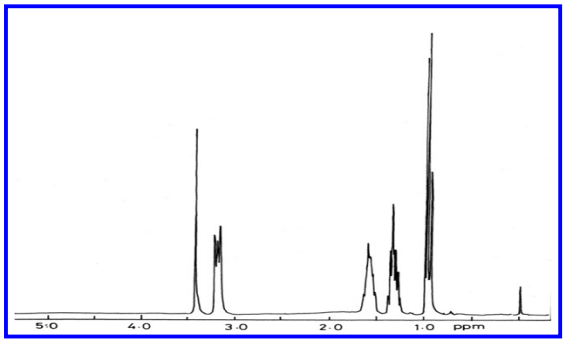

Fig. 3 ^{1}H NMR spectrum of TBATBr-Co(II)

3.4 ^{13}C NMR Spectral Analysis

The ^{13}C NMR spectrum of TBATBr-Co(II) was recorded in AVANCE III 500 MHz Bruker Facility. In TBATBr-Co(II) compound, apart from the signals caused by two identical methyl carbon atoms of DMSO, there are four signals observed (Fig. 4.). Since nitrogen has positive charge in the tetrabutylammonium group of the compound, there is more deshielding for the carbon atom nearer to the nitrogen atom. This deshielding in the carbon atoms diminishes as we move further away from the nitrogen atom leading to a decrease in the δ values consequently. Hence the methylene carbon nearer to the nitrogen atom has a higher δ value of 57. For the second methylene carbon atom from the nitrogen atom the δ value is 22. For the third methylene carbon atom from the nitrogen atom the δ value decreases further leading to 18. Since the methyl group carbon atom is far away from the positively charged nitrogen atom the deshielding effect is very minimum leading to a δ value of 13. Though there are four N-butyl groups in the tetrabutylammonium group only four signals for four different carbon atoms are observed. This leads to the conclusion that all the eight N-butyl groups are identical.

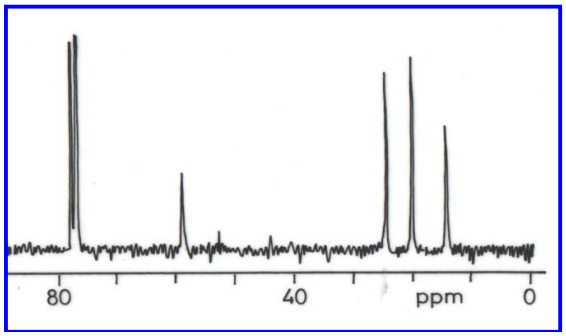

Fig. 4: ^{13}C NMR spectrum of TBATBr-Co(II)

3.5 Powder XRD

The X-ray powder diffraction pattern of TBATBr-Co(II) was carried out using Bruker AXS D8 diffractometer. The X-ray powder diffraction pattern spectrum is shown in Fig 5. The X- ray pattern shows well defined Bragg peaks at specific 2θ angles which reveal that the sample is crystalline with good quality. The 2θ and d values are tabulated in Table 3.

Table 3. X- ray powder diffraction data of TBATBr-Co(II)

Pos. [°2Th.]	Height [cts]	FWHM [°2Th.]	d-spacing[Ao]	Rel. Int. [%]
10.3530	207.94	0.2007	8.54470	100.00
10.7021	130.74	0.3011	8.26677	62.88
11.3898	173.16	0.2676	7.76911	83.27
12.2217	170.41	0.3346	7.24208	81.95
15.5877	70.18	0.2676	5.68501	33.75
16.0047	40.69	0.1673	5.53780	19.57
17.6146	29.77	0.2342	5.03512	14.32
18.0957	38.83	0.2007	4.90233	18.67
19.3209	33.38	0.3011	4.59414	16.05
19.6826	122.98	0.2342	4.51052	59.14
20.6263	44.34	0.3011	4.30624	21.33
21.6749	127.61	0.2342	4.10021	61.37
22.0285	98.59	0.2676	4.03519	47.41
22.6885	44.61	0.2676	3.91929	21.45
23.0762	71.25	0.3178	3.85430	34.26
23.8983	143.38	0.2676	3.72355	68.95
24.3674	146.15	0.3680	3.65293	70.28
25.1245	131.07	0.2007	3.54454	63.03
25.6819	54.14	0.2676	3.46885	26.04
26.0631	101.97	0.3346	3.41898	49.04
26.9141	43.46	0.2676	3.31278	20.90
27.2477	96.14	0.2342	3.27297	46.23
28.9479	25.82	0.2676	3.08449	12.42
30.6781	93.70	0.2175	2.91437	45.06
32.1503	69.69	0.3346	2.78419	33.51
32.8055	35.25	0.2007	2.73006	16.95
33.6251	129.07	0.3011	2.66538	62.07
35.3443	31.74	0.4015	2.53957	15.26
37.0925	24.52	0.4015	2.42380	11.79
38.4672	19.80	0.5353	2.34028	9.52
39.5196	21.16	0.2676	2.28036	10.18
42.6390	47.62	0.3346	2.12047	22.90
44.5163	61.23	0.3346	2.03531	29.45
45.8970	33.73	0.8029	1.97725	16.22
55.7208	59.60	0.5353	1.64970	28.66
68.5568	15.63	0.4080	1.36768	7.52

The structure of the compound was determined as monoclinic with space group $P2_1/n$ with the unit cell dimensions, a = 16.5255Å, b = 15.5263Å. c = 18.6371Å with Z = 4. The co-ordination around Co atom is tetrahedral. The structure of the compound also shows hydrogen bonds between bromide and hydrogen of the butyl groups.

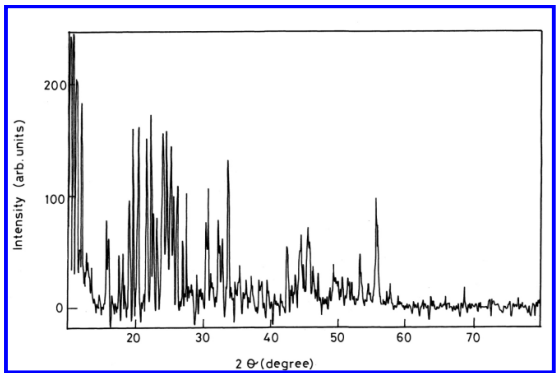

Fig. 5: X- ray powder diffraction pattern of TBATBrCo(II)

3.6 Single crystal X-Ray structural analysis

The structure of the compound was determined by using single crystal X-ray diffraction technique. The X-ray data is collected at 293K using the M_oK_α radiation ($\lambda = 0.71073A^o$). A good quality bluish green colour single crystal of size 0.10x0.10x0.20 mm is used for collecting data. The structure was solved by direct methods using the program SHELXS97 and refined on F^2 by full-matrix least-squares procedures using the program SHELXL97[21]. The non-hydrogen atoms were refined anisotropically and the hydrogen atoms were constrained to ride on their respective parent atoms. The geometrical parameters and the figures were done using the programs PARSTand PLATON. The compound crystallizes in monoclinic space group $P2_1/n$ and its unit cell parameters are found to be, a = 16.5255(5)Å, b = 15.5263(4)Å, c = 18.6371(5)Å and $\beta = 116.027(1)^\circ$. The structure was solved with the final reliability index value of 0.0405. The crystal data of TBATBr – Co(II) is presented in Table 4.

The ORTEP plot of theTBATBr-Co(II) molecule in Fig. 6. The structure of TBATBr-Co(II) compound has eight butyl groups. Due to the bulky butyl groups, the molecule is under high stress. Due to the stress and strain, one of the butyl groups (C5-C6-C7-C8) does not able to fit in a position. Thus disorder exists in the compound and C5-C6-C7-C8 butyl group is wagging between positions C7A, C8A and C7B, C8B. Atomic coordinates and its equivalent isotropic displacement parameters involving non-hydrogen atoms for TBATBr-Co(II) is listed in Table 5. The C-N bond length is observed for all carbon atoms interacting with both the nitrogen atoms (N1 & N2) and found to be in the range of 1.504(5)Å-1.520(6)Å (Table 6). This is shorter than the normal bond length value 1.57Å, which proves that the C-N bond is stronger than expected. In the $CoBr_4$ tetrahedra group, bond length ranges from 2.403(8)Å to 2.418(8)Å for all the Co-Br bonds. The Co-Br bond length is greater, when compared to C-N and C-C bond lengths (Table 6). Usually the metal-halogen bonds are weaker and hence they have higher bond lengths.

Table 4. Crystal data for TBATBr-Co(II)

Parameters	TBATBr-Co(II)
CCDC	1019224
Empirical formula	C32 H72 Br4 Co N2
Formula weight	863.49
Temperature(K)	293(2)
Wavelength(Å)	0.71073
Crystal system	Monoclininc
Space group	P21/n
Unit cell dimensions	
a(Å)	16.5255(5)
b(Å)	15.5263(4)
c(Å)	18.6371(5)
β(°)	116.0270(10)
Volume(Å3)	4297.0(2)
Z	4
Calculated density(Mg/m3)	1.335
F(000)	1780
Crystal size(mm)	0.10 x 0.10 x 0.20
θ - range for data collection(°)	1.38 to 25.58
Limiting indices	-20<=h<=19
	-18<=k<=18
	-22<=l<=22
Reflections collected / unique	41923 / 8040
	[R(int) = 0.0540]
Completeness to θ = 25.00(%)	99.5
Refinement method	Full-matrix least-squares on F2
Data / restraints / parameters	8040 / 3 / 379
Goodness-of-fit on F2	1.081
Final R indices [I>2σ(I)]	R1 = 0.0405, wR2 = 0.0945
R indices (all data)	R1 = 0.1028, wR2 = 0.1168
Largest diff. peak and hole(eÅ-3)	0.514 and -0.430

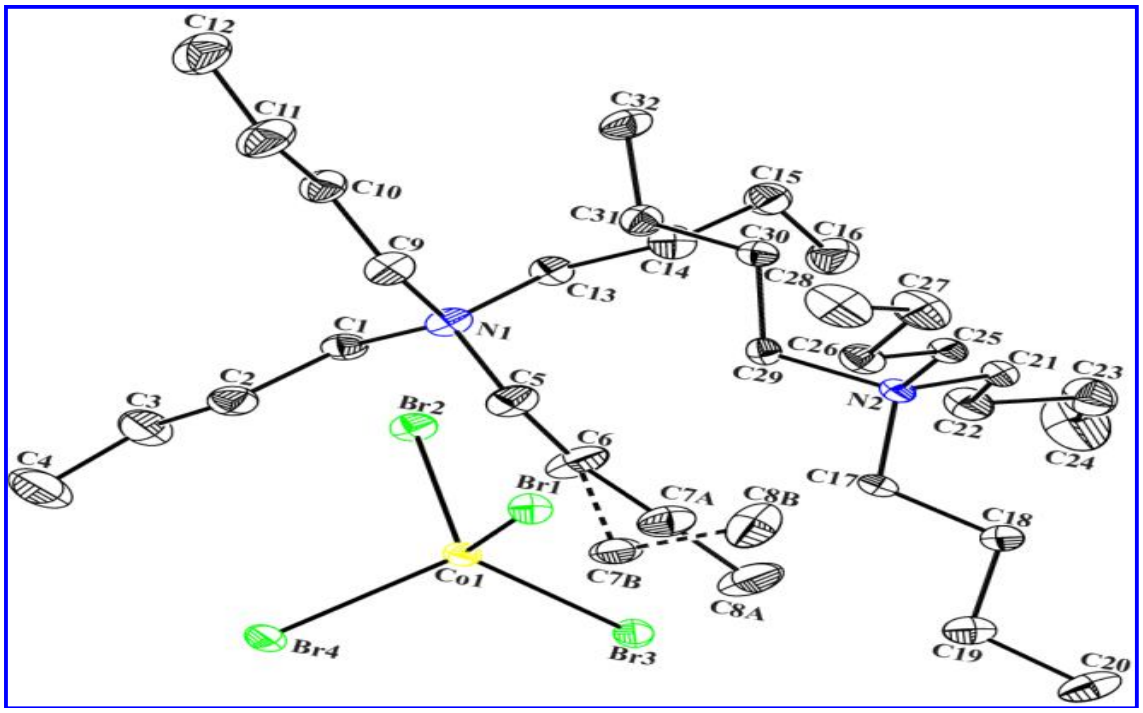

Fig. 6: ORTEP plot of TBATBr–Co(II)

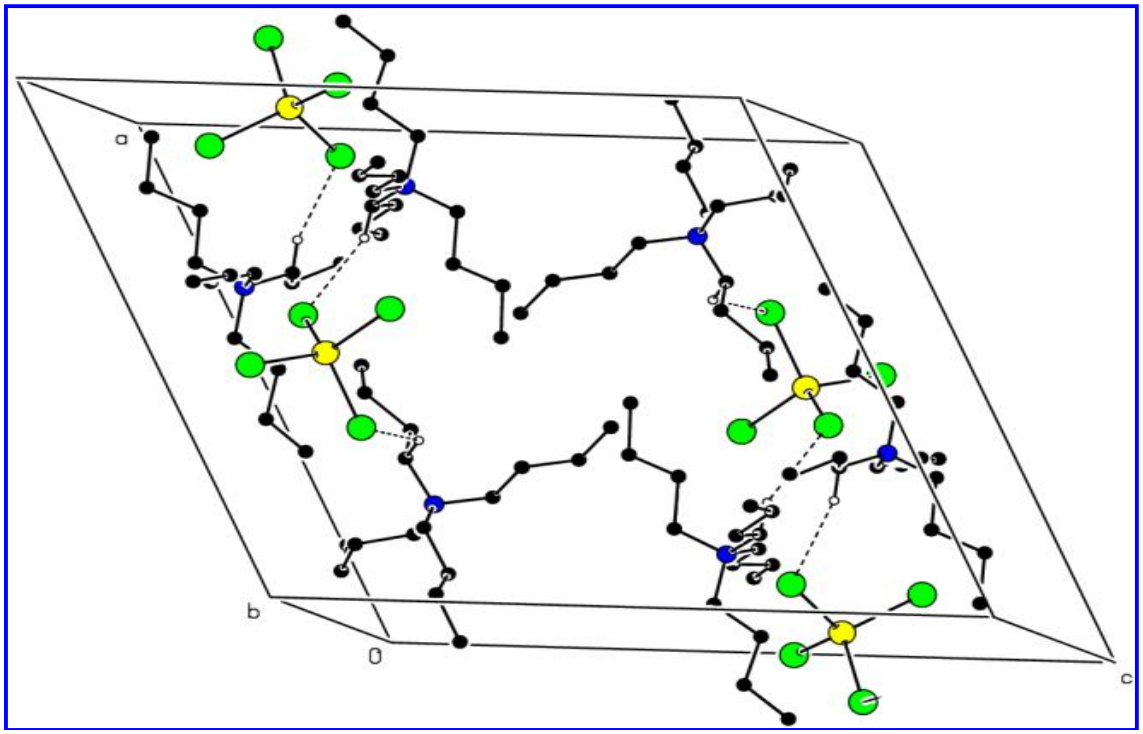

Fig. 7: The crystal packing of the molecules in compound TBATBr–Co(II). H atoms which are not involved in hydrogen bonding have been omitted for clarity

Table 5. Atomic coordinates (x104) and equivalent isotropic displacement parameters (2x103) involving non-hydrogen atoms for TBATBr-Co(II)

Atoms	x	y	z	U(eq)*
N1	2265(3)	5581(2)	2320(2)	75(1)
C1	2459(3)	5258(3)	3142(3)	77(1)
C2	3015(4)	5821(4)	3835(3)	101(2)
C3	3228(5)	5353(5)	4618(4)	130(2)
C4	3847(5)	5783(6)	5351(4)	188(4)
C5	3131(4)	5762(3)	2256(4)	97(2)
C6	3749(4)	5012(4)	2421(5)	135(3)
C7A	4426(15)	5320(20)	2075(13)	149(9)
C8A	5019(10)	4578(13)	2113(13)	184(7)
C9	1737(4)	6409(3)	2130(3)	93(2)
C10	846(4)	6367(3)	2149(3)	99(2)
C11	379(6)	7231(5)	1961(5)	150(3)
C12	-539(6)	7171(6)	1960(5)	181(4)
C13	1725(3)	4881(3)	1735(3)	76(1)
C14	1486(4)	5034(4)	863(3)	98(2)
C15	1021(4)	4264(4)	379(3)	103(2)
C16	1596(5)	3497(5)	535(4)	137(3)
C7B	4711(17)	5250(30)	2524(11)	107(7)
C8B	4500(30)	5210(20)	1634(19)	179(12)
N2	3323(2)	7769(2)	-682(2)	63(1)
C17	4317(3)	7893(3)	-178(2)	70(1)
C18	4910(3)	7747(4)	-598(3)	88(2)
C19	5876(4)	7947(4)	-57(4)	105(2)
C20	6503(4)	7747(5)	-418(5)	142(3)
C21	3127(3)	6873(3)	-1041(3)	75(1)
C22	3380(4)	6135(3)	-472(3)	100(2)
C23	3300(5)	5294(4)	-908(4)	131(2)
C24	3509(8)	4535(5)	-452(5)	219(5)
C25	2968(3)	8396(3)	-1367(2)	72(1)
C26	3084(4)	9336(3)	-1161(3)	89(2)
C27	2634(5)	9868(4)	-1903(4)	133(3)
C28	2618(5)	10798(5)	-1768(4)	157(3)
C29	2864(3)	7905(3)	-143(2)	68(1)
C30	1841(3)	7930(3)	-564(3)	79(1)
C31	1433(4)	7773(4)	3(3)	97(2)
C32	430(4)	7902(5)	-391(4)	139(3)
Br1	458(1)	4770(1)	3722(1)	80(1)
Br2	1481(1)	3034(1)	2836(1)	81(1)
Br3	-731(1)	2472(1)	2958(1)	83(1)
Br4	-750(1)	4284(1)	1448(1)	88(1)
Co1	89(1)	3640(1)	2739(1)	60(1)

Table 6. Selected bond lengths (Å) of TBATBr-Co(II)

Atoms	Lengths	Atoms	Lengths
N1-C9	1.507(6)	N2-C17	1.505(5)
N1-C1	1.508(6)	N2-C29	1.515(5)
N1-C5	1.513(6)	N2-C21	1.517(6)
N1-C13	1.520(6)	C17-C18	1.515(6)
C1-C2	1.496(7)	C18-C19	1.499(7)
C2-C3	1.526(8)	C19-C20	1.494(8)
C3-C4	1.460(8)	C21-C22	1.490(7)
C5-C6	1.489(8)	C22-C23	1.513(8)
C6-C7B	1.56(3)	C23-C24	1.405(9)
C6-C7A	1.59(3)	C25-C26	1.500(6)
C7A-C8A	1.50(4)	C26-C27	1.498(7)
C9-C10	1.489(7)	C27-C28	1.467(8)
C10-C11	1.511(8)	C29-C30	1.520(6)
C11-C12	1.519(10)	C30-C31	1.502(6)
C13-C14	1.514(6)	C31-C32	1.503(8)
C14-C15	1.491(7)	Br1-Co1	2.4141(7)
C15-C16	1.471(8)	Br2-Co1	2.4177(8)
C7B-C8B	1.54(4)	Br3-Co1	2.4033(8)
N2-C25	1.504(5)	Br4-Co1	2.4046(7)

Table 7. Selected bond angles (°) of TBATBr-Co(II)

Atoms	Angles	Atoms	Angles
C9-N1-C1	111.4(4)	C17-N2-C29	107.2(3)
C9-N1-C5	107.0(4)	C25-N2-C21	106.9(3)
C1-N1-C5	110.8(4)	C17-N2-C21	110.9(4)
C9-N1-C13	110.2(4)	C29-N2-C21	110.4(3)
C1-N1-C13	106.7(3)	N2-C17-C18	115.8(3)
C5-N1-C13	110.8(4)	C19-C18-C17	111.2(4)
C2-C1-N1	117.4(4)	C20-C19-C18	113.5(5)
C1-C2-C3	110.1(5)	C22-C21-N2	116.8(4)
C4-C3-C2	116.7(6)	C21-C22-C23	110.5(5)
C6-C5-N1	115.2(4)	C24-C23-C22	117.4(7)
C5-C6-C7B	114.4(15)	C26-C25-N2	117.0(4)
C5-C6-C7A	102.7(13)	C27-C26-C25	110.2(4)
C7B-C6-C7A	28.2(9)	C28-C27-C26	115.1(6)
C8A-C7A-C6	108(2)	N2-C29-C30	115.4(4)
C10-C9-N1	115.7(4)	C31-C30-C29	112.0(4)
C9-C10-C11	111.4(5)	C30-C31-C32	111.9(5)
C10-C11-C12	110.7(7)	Br1-Co1-Br2	108.09(3)
C14-C13-N1	116.9(4)	Br3-Co1-Br4	111.28(3)
C15-C14-C13	110.2(4)	Br3-Co1-Br1	113.12(3)
C16-C15-C14	114.4(5)	Br4-Co1-Br1	107.46(3)
C8B-C7B-C6	97(2)	Br3-Co1-Br2	106.45(3)
C25-N2-C17	111.1(4)	Br4-Co1-Br2	110.39(3)
C25-N2-C29	110.5(3)		

The bond angles of theTBATBr – Co(II) molecule are given in Table 7. The bond angles of Br-Co-Br deviate from the normal tetrahedral angle indicating that compression and expansion of bonds. This may be due to the interaction between hydrogen atoms of nearby butyl groups and bromine atoms in the $CoBr_4$ groups. The remark of the bond angles among N1-C1-C2, N1-C13-C14, N2-C21-C22 and N2-C25-C26 is around 117° and bond angles among N1-C5-C6, N1-C9-C10, N2-C29-C30 and N2-C17-C18 is more or less 115°, which depicts that these bonds are in structurally identical positions. The hydrogen bonds present between the hydrogens of the butyl groups and halogen atoms of the $CoBr_4$ group leads to a stronger interaction between the two N-butyl groups and bromine co-ordinated metal atom Co (Table 8). The packing of the molecule TBATBr – Co(II) is presented in Fig. 7.

Table 8. Hydrogen bonding geometry (Å and °) for TBATBr-Co(II)

D-H…A	d(D-H)	d(H..A)	d(D..A)	∠(DHA)
C5-H5B...Br_2 a	0.97(5)	2.964	3.603(5)	124.51(32)
C25-H25B...Br_3b	0.97(4)	2.918(1)	3.827(4)	156.51(28)

Symmetry codes: (a) -x+1/2,+y+1/2,-z+1/2 (b) -x,-y+1,-z

3.7 Thermal analysis

The TG and DTG curves of TBATBr-Co(II) crystals are given in Fig.8. The TG-DTG curve shows a two stage weight loss when heated between 40 ºC and 800 ºC. The first stage decomposition starts at 253 ºC and ends at 370 ºC. There is a weight loss of 70% which can be accomplished by formulating the following, decomposition reaction of the compound.

$$\underset{863}{[N(C_4H_9)_4]CoBr} \longrightarrow \underset{644}{2N(C_4H_9)_4Br\uparrow} + \underset{219}{CoBr_2}$$

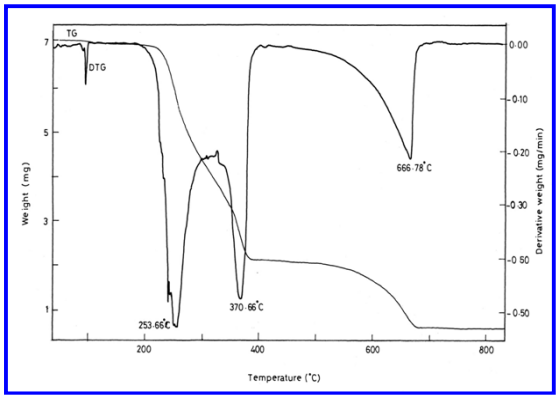

Fig. 8: TG/TDA spectrum of TBATBr-Co(II)

When the compound undergoes decomposition as above, one mole of the compound decomposes into two moles of tetrabutylammonium bromide and one mole of cobalt bromide. Since cobalt bromide is stable at these temperatures it does not vaporise. Only the tetrabutylammonium bromide vaporises at this temperature leads to the loss of 644 units for two moles of the compound. Theoretical weight loss of 74.6 % is observed whereas the experimental loss observed is 70 %. The difference of 4.6 % may be attributed to the incomplete decomposition of small amount of the compound. In the second stage we have only cobalt bromide at 370 ºC. When the temperature is increased there is decomposition of cobalt bromide from 370 ºC to 666 ºC with a weight loses of 22%. This weight loss can be accounted by formulating the following decomposition reaction.

$$\underset{219}{CoBr_2} \longrightarrow \underset{69}{Co\downarrow} + \underset{160}{Br_2\uparrow}$$

According to the above equation, cobalt bromide has completely decomposed into gaseous bromine and cobalt residue. Thus there is loss of all the 219 units of cobalt bromide into cobalt residue and of gaseous bromine. The theoretical loss of weight of 160 units leads to the loss of 18.5 % of the original compound. The difference of 3.5 % between the theoretical and experimental value is due to the decomposition of small amount of the TBATBr-Co(II) left in the first stage. Thus the compound decomposes in two stages. The decomposition starts at 253 ºC and gets completed at 667 ºC. The melting point of cobalt is 1495 ºC. So cobalt remains as residue after the second stage of decomposition. It does not vapourise even after 836 ºC. Here, the theoretical percentage value of cobalt residue is 6.84. The experimental percentage value is 8. The experimental and theoretical values are in agreement with each other with a difference of 1.16 % which is within experimental error. Thus the thermogram confirms the stoichiometry of the compound which is evident from the decomposition patterns.

The DTG curve of the cobalt compound involves four peaks. They occur at temperatures 98.3º, 253.6º, 370.6º and 666.7 ºC. The 98.3 ºC peak is attributed to the presence of moisture in the crystal which lost at this temperature. The first stage of decomposition occurs between 253.6º and 370.6 ºC. The second stage of decomposition occurs between 370.6º and 666.7 ºC. Thus the TG and DTG curves agree with each other for the decomposition pattern of the compound. The low temperature DSC curves

(Fig. 9a & Fig. 9b) show one sharp and another very sharp endothermic peak when the experiment was carried out between 100 ºC and 240 ºC. The sharp peak starts at 53.54 ºC and ends at 64.4 ºC and the peak temperature is 59.9 ºC. The onset of the very sharp peak is at 95.38 ºC and the endset at 100.4 ºC. The peak temperature is 98.3 ºC. These two peaks indicate that the crystal shows one phase transition at 59.9 ºC and another at 98.3 ºC on the high temperature side. A glass transition temperature is observed at -84.8 ºC. The glass transition is about to onset at -90ºC. High temperature DSC curve of cobalt compound shows only one major peak at 268.6º in Fig.10. The other two minor peaks are observed at 71.8 ºC and 99.1 ºC with low enthalpy values. This is due to the evaporation of less amount of moisture present in the crystal. The major peak at 268.4 ºC indicates the decomposition of compound at this temperature which is an evident from the DTG thermogram. For the decomposition process the enthalpy value is 64.09 kj/mol.

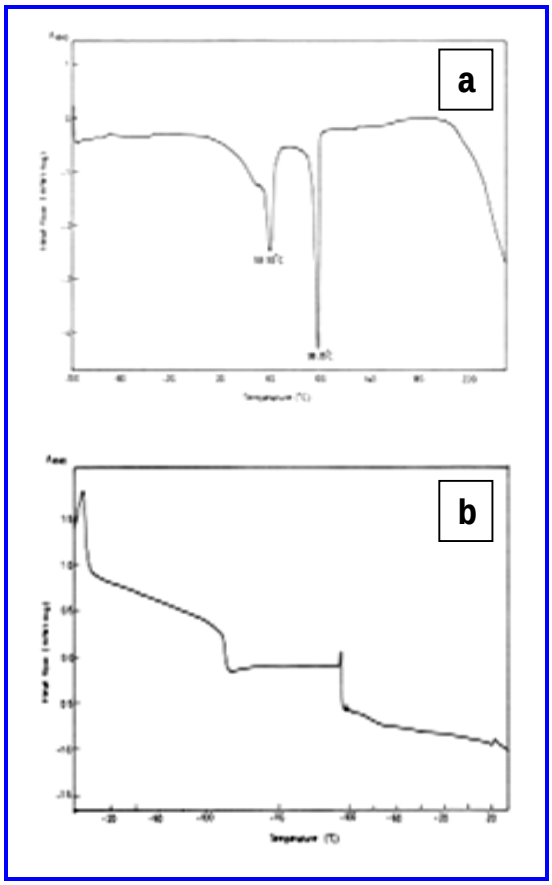

Fig. 9(a) & 9(b) : Low temperature DSC curves of TBATBr-Co(II)

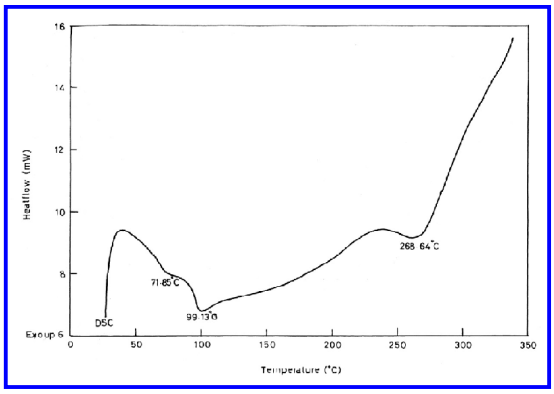

Fig: 10: High temperature DSC of TBATBr-Co(II)

4. CONCLUSION

Single crystals of TBATBr-Co(II) crystals were grown from saturated solutions by means of slow evaporationmethod at room temperature. The grown crystals were characterized using elemental analysis, Single crystal X-ray diffraction, powder X-ray diffraction, thermal analysis, NMR, and FTIR studies. The elemental analysis of the compound conform the stoichiometric ratio. The sharp and well-defined Bragg peaks obtained at specific 2θ angles for the crystals confirm the crystalline nature of the compound. The decomposition pattern of the compound was formulated based on the TG thermogram. The weight losses observed in the TG curves of the compound, fit well with the formulated decomposition pattern. The DTA was also carried out. Various kinds of protons and carbons present in the crystals were confirmed by NMR spectroscopic technique and various absorption frequencies in FTIR spectroscopy. The structure and crystal packing of the compound is obtained through single crystal X-ray diffraction data. The crystal has been confirmed and this material can be a used to thermal stability of optical applications. This study may be helpful to design new metal complexes with technical applications

ACKNOWLEDGEMENT

One of the author MT acknowledge the financial support from SASTRA University, Thanjavur, TN, India, under Prof. T. R. Rajagopalan research fund.

REFERENCES

Amirthaganesan, G., Kandhaswamy, M. A. and Srinivasan, V., Synthesis, characterization and structural phase transition studies in trismethylammoniumpentachloro barium dihydrate single crystals, *Cryst. Res. Technol.*, 38(10), 910-912 (2003). doi:10.1002/crat.200310111

Byrappa, K., Kandhaswamy, M. A. and Srinivasan,V., Growth, Morphology, Structure and Properties of Na_3BaCl_5 $2H_2O$ Crystals, *Cryst. Res. Technol.*, 34(7), 143-150(1999). doi:10.1002/(SICI)1521-4079(199908)34:7 <843 ::AID-CRAT843 >3.0.CO;2-W

Eychmuller, A., Rogach, A. L., Chemistry and photophysics of thiol-stabilized II-VI semiconductor nanocrystals, *Pure Appl. Chem.*, 72(1), 179-188(2000). doi:10.1351/pac200072010179

Iwata, M., and Ishibashi, Y., Dielectric dispersion in $[N(C_2H_5)_4]2ZnCl_4$ Single Crystal, *Lett*, 60(10), 3245-3248(1991). doi:10.1143/JPSJ.60.3245

Kahrizi, M. and M. O., Steinitz Solid State Communication, *Sciencedirect*, 74(5), 333-335, (1990). doi:10.1016/0038-1098(90)90497-Y

Koopmans, B., Anema, A., Jonkman, H. T., Sawatzky, G. A. and Van der Woude, F., Resonant-optical-second-harmonic generation from thin C60 films, *Phys. Rev.*, 48(4), 2759-2770 (1993). doi:10.1103/PhysRevB.48.2759

Koopmans, B., Janner, A. M., Jonkman, H. T., Sawatzky, G. A. and Van der Woude, F., Strong bulk magnetic dipole induced second-harmonic generation from C60, *Phys. Rev. Lett.*, 71(21), 3569-3580(1993). doi:10.1103/PhysRevLett.71.3569

Maurya, R. C., Sharma, P., Roy, S., Synthesis and characterization of some mixed-ligand picrate complexes of Nickel(II) involving heterocyclic nitrogen donors, *Synth. React. Inorg. Metal. Org. Chem.*, 33(4), 683-698 (2003). doi:10.1081/SIM-120020332

Moore, C. M. S., Hackman, Brennan, T. and Minteer, S. D., Effect of mixture casting phosphonium salts with Nafion® on the proton exchange capacity and mass transport through the membranes, *J. Membr. Sci.*, 254(1), 63-70 (2005). doi:10.1016/j.memsci.2004.11.027

Petrosyan, H. A., Karapetyan, H. A., Yu Antipin, M., Petrosyan, A. M., Nonlinear optical crystals of l-histidine salts, *J. Cryst. Growth*, 275(1), 1919-1925(2005). doi:10.1016/j.jcrysgro.2004.11.258

Sawada, S., Takashige, M., Shimizu, F., Suzuki, H., and Yamaguchi, T., Ferroelectricity in A 2 BX 4-type halide compounds, *Ferroelectrics*, 169(1), 207-214 (1995). doi:10.1080/00150199508217331

Shuai, Z., Brédas, Magnetic dipole and electric quadrupole contributions to second-harmonic generation in C60—A valence effective hamiltonian study, *J. L., Adv. Mater*, 6(6), 486-488 (1994). doi:10.1002/adma.19940060610

Xue, D., Ratajczak, H., Effect of hydrogen bonds on physical properties of ammonium dihydrogenphosphate crystals, *J. Mol. Struct.*, 716(1), 207-210(2005). doi:10.1016/j.theochem.2004.11.026

Young Kim, D., Kwun, S., Gul Yoon, Linear birefringence behavior of A2BX4-type ferroic crystals in the normal-incommensurate phase transition, *J., Phys. Rev.*, 57(18), 11173-11185 (1998b).doi:10.1103/PhysRevB.57.11173